

pubs.acs.org/JPCC Article

Operando XPS for Plasma Process Monitoring: A Case Study on the Hydrogenation of Copper Oxide Confined under h-BN

J. Trey Diulus,* Andrew E. Naclerio, Jorge Anibal Boscoboinik, Ashley R. Head, Evgheni Strelcov, Piran R. Kidambi, and Andrei Kolmakov*



Cite This: J. Phys. Chem. C 2024, 128, 7591-7600



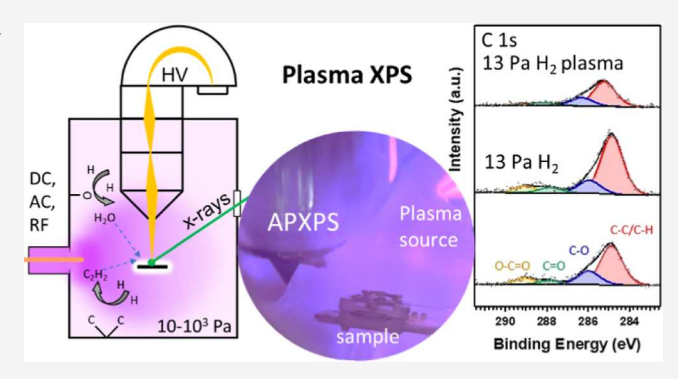
ACCESS I

III Metrics & More

Article Recommendations

sı Supporting Information

ABSTRACT: We demonstrate that ambient pressure X-ray photoelectron spectroscopy (APXPS) can be used for in situ studies of dynamic changes in surface chemistry in a plasma environment. This opens a new and vast application space for XPS and greatly complements modern spectroscopy techniques to probe plasma—solid/liquid interactions relevant to process monitoring in the semiconductor industry, biomedical plasma applications, and plasma remediation technologies. Hexagonal boron nitride (h-BN) grown on Cu was used in this study as a well-defined model system for plasma process monitoring because of its unique chemical, optical, and electrical properties that make it a prospective material for advanced electronics. To better understand the stability and surface chemistry of h-BN during plasma-



assisted processing, we track in real time the plasma-induced chemical state changes of B, N, and the underlying Cu substrate using APXPS equipped with an AC discharge plasma source operating at 13 Pa. Residual gas analysis mass-spectra were concurrently collected during plasma-XPS to track reaction products formed during plasma exposure. A clear reduction of Cu_xO is seen, while an h-BN layer remains intact, suggesting that hydrogen radical (H $^{\bullet}$) species can attack the exposed and h-BN-covered Cu oxide patches and partially reduce the underlying substrate without significantly damaging the overlaying h-BN, which is of practical importance for development of h-BN-encapsulated devices and interfaces. In addition to demonstration of plasma-XPS capabilities, we discuss the observed challenges (e.g., parasitic plasma-chamber wall reactions and charging effects) and propose potential solutions.

1. INTRODUCTION

Modern ambient pressure X-ray photoelectron spectroscopy (APXPS) measurements are conducted at pressures spanning approximately 10^{-8} to 10^3 Pa range, allowing for a robust metrology technique of choice for in situ studies of realistic surfaces and interfaces, specifically for gas-solid or gas-liquid interfacial reactions (see recent reviews1-3 and references therein). There is a clear recent trend in the application of APXPS to operando studies relevant to semiconductor microfabrication technologies.4 In this regard, most cold plasma semiconductor processing occurs at 10^{-1} to 10^3 Pa, which overlaps with the operational pressure range for APXPS. Therefore, application of APXPS to interrogate the surfaces and interfaces in a plasma environment is, in principle, possible. This would be greatly beneficial for fundamental studies of plasma-solid/liquid interactions (see recent perspectives^{5,6} and references therein) and plasma-assisted process monitoring in semiconductor fabrication technology, where the real-time analysis of interfacial chemical composition with submonolayer precision is a common requirement. The original solution for quasi-real-time monitoring of plasmasurface interaction using electron spectroscopy employed the

so-called "spinning wall" method.⁷ This involves a fast-rotating cylindrical sample positioned between two differentially pumped skimmers; thus, the sample can be exposed to a plasma environment at one side and can be probed with Auger electron spectroscopy and mass spectrometer from the other high-vacuum side up to ca. millisecond after plasma exposure. However, to our best knowledge, no systematic efforts have been undertaken yet, except for a recent application note, 8 to collect true real-time XPS spectra under plasma operating conditions. Instead, a traditional ex situ or in situ (without vacuum breaking) "before-and-after" plasma exposure approach is usually employed.^{9,10} Both methods are suitable for understanding many plasma-induced surface phenomena but lack the ability to track short-living or fast-diffusing chemical intermediates that may control reaction mechanisms at the

Received: January 12, 2024 Revised: April 10, 2024 Accepted: April 12, 2024 Published: April 29, 2024





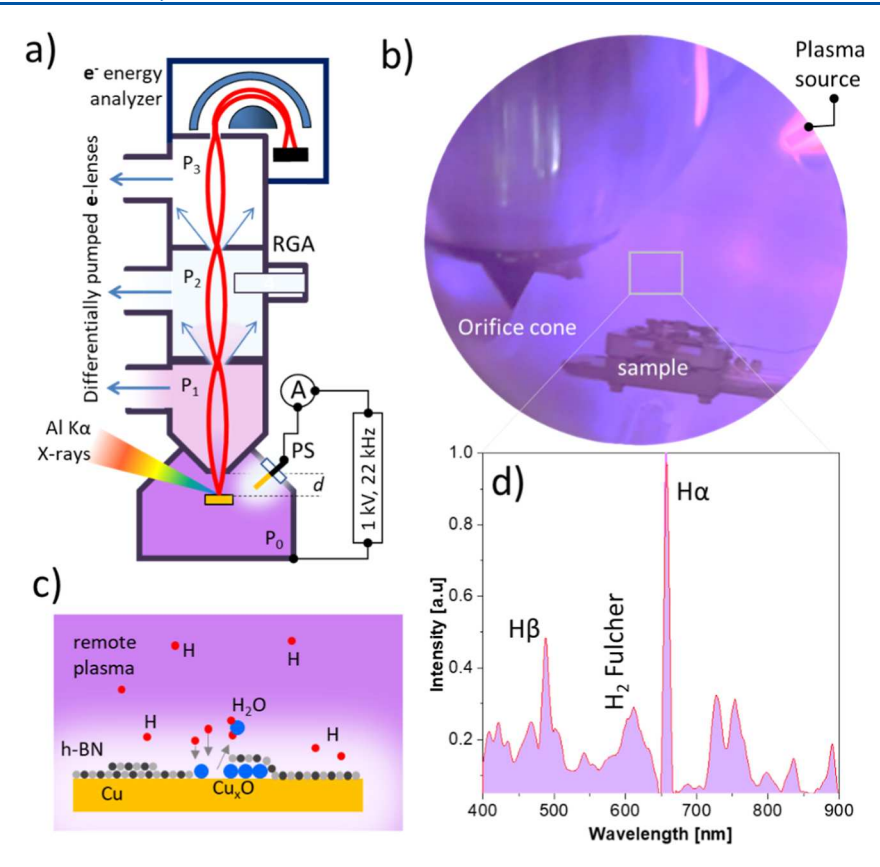


Figure 1. Schematic of BNL APXPS system with the reaction chamber, plasma source (PS), and residual gas analyzer (RGA) (a); photograph of the ignited plasma at 13 Pa (b) with the sample retracted away from XPS focus; diagram of plasma surface interaction for h-BN/Cu (c); remote H₂ plasma emission spectrum (wide slits) collected near the sample also at 13 Pa (d).

plasma—solid, plasma—liquid, or bio-interfaces. Moreover, many processes, such as plasma-assisted atomic layer deposition and pulsed plasma etching, employed in semiconductor manufacturing are inherently time-dependent, thus requiring *operando* surface status diagnostics. Here, we demonstrate laboratory-based APXPS capabilities for studying plasma-induced surface chemistry and confined reactions *in operando*, using a hexagonal boron nitride (h-BN) monolayer grown via chemical vapor deposition (CVD) on polycrystalline Cu foils as a model system.

h-BN has garnered significant interest in the advanced electronics community due to a wide array of unique chemical, thermal, and electrical properties that are useful in numerous optical and electronic applications (see reviews in refs 11-13 and references therein). h-BN-capped heterostructures and interfaces have been of interest for solid-state lighting, highpower/temperature electronics, etc. Due to a wide bandgap of about ≈6 eV, chemical inertness, and breakdown strength, h-BN has also been suggested as a prospective trap-free gate dielectric material, showing particularly impressive performance in 2D electronics and high-mobility diamond transistors. 14 Multiple studies have shown that h-BN can further act as a passivation layer, to resist complete oxidation of an underlying substrate¹⁵ or impede interlayer diffusion through stacked materials in electronic devices. 16 Cu is a convenient model substrate material for testing boron nitride as an encapsulant because h-BN can be epitaxially grown via CVD on any Cu orientation, with a near-perfect lattice match achievable on the Cu(111) surface. 11 Furthermore, the

synthesis/transfer of h-BN/Cu to arbitrary substrates can routinely be done using a variety of wet or dry methods. 17,18

An ideal CVD-grown, defect-free single-crystal h-BN layer would completely prevent the oxidation of the Cu substrate. However, intercalation of O2 through the point/linear defects in an h-BN monolayer can still occur in realistic samples, yielding an underneath Cu surface predominantly oxidized to copper(I) oxide (Cu₂O) instead of complete oxidation to copper(II) oxide (CuO). This intercalative oxidation can occur thermodynamically, even at room temperature (RT), if the partial pressure of oxidizing species is high enough. This can limit the lifetime of pristine unoxidized h-BN/Cu heterostructures to a few weeks in an ambient environment. 19-21 In addition to intercalative oxidation, deintercalation has also been demonstrated, 19 although the ability to subsequently intercalate a reducing molecule and recover the initial interface without completely destroying the h-BN layer has been more challenging to achieve.

Transport through 2D membranes is well known and has been suggested as a method for improvement across several electronic applications.²² Prior H₂ exposure experiments to intercalate molecular hydrogen under h-BN showed that the process can occur either through the defects or via edge intercalation at the h-BN/Cu interface due to the low energy barrier for molecular dissociation and diffusion at the interface.²³ On the other hand, plasma-generated hydrogen radicals (H•) have an atomic diameter smaller than the h-BN lattice constant and can potentially penetrate directly through the hexagonal ring, thus increasing the probability of reacting with the underneath substrate. A previous report²⁴ shows that

not only can remote plasma H^{\bullet} radicals intercalate through h-BN but can also form hydrogen "bubbles" after intercalation due to recombination of radicals underneath the h-BN. Interestingly, exposure to an Ar and O_2 plasma does not show such behavior, supporting the radical/ion size selectivity of the intercalation process. The reaction and modification of the h-BN itself due to reaction with hydrogen radicals has been reported as well. ^{25–28}

Overall, the understanding of plasma-induced surface and interfacial (e.g., intercalation) reactions is still elusive and would greatly benefit from operando plasma-XPS capabilities that are demonstrated and discussed in this report. Using polycrystalline Cu foils with CVD-grown h-BN that have been slightly oxidized in ambient conditions as a model system, we comparatively assessed the reduction at RT of the surface via two hydrogenation methods: (i) simple exposure to H₂ at 13 Pa and (ii) exposure to a low-power (15 W) H₂ remote plasma also at 13 Pa with APXPS. Complementary scanning electron microscopy (SEM) provides morphological maps of foil surfaces before and after hydrogen radical exposure. Using plasma-XPS, and a sample with a 2D overlayer, we demonstrate the ability to track dynamic changes related to plasma-induced chemistry. Ultimately, we show that H^o can interact with the confined oxide and reduce the Cu surface, suggesting that a route to reduce the Cu substrate and recover the original h-BN/Cu interface is possible within a certain parameter space.

2. METHODS

Single monolayer h-BN was grown on polycrystalline Cu foil via CVD using a low-pressure chemical vapor deposition (LPCVD) setup. 11 Briefly, polycrystalline Cu foil (99.9% purity, 18 μ m thick) is pre-etched in 20% nitric acid to remove surface contaminants, followed by successive water rinses. After drying, the sample is loaded into a custom LPCVD system consisting of a hot-walled tube furnace with a separate side chamber up-stream of the reactor in which the solid precursor (ammonia-borane, 98% purity) is sublimed. The foil is annealed for 30 minutes at 1025 °C under 500 sccm of hydrogen prior to growth. h-BN is grown at 1025 °C under 50 sccm of hydrogen by subliming 3.5 mg of ammonia-borane precursor at 85 °C for 90 min. The precursor supply is then cut off and the reactor is rapidly quenched to room temperature. The h-BN/Cu samples were briefly exposed to the atmosphere following deposition and then stored in vacuum (ca. ≈10 Pa) inside a desiccator box for a few months, where they have gotten slightly oxidized, predominantly at the defect sites. We used these h-BN/Cu samples as a model system for studying the H[•]-induced recovery of the original metallic Cu at the h-BN interface.

Plasma-XPS experiments were performed at the Center for Functional Materials at Brookhaven National Laboratory equipped with a lab-based APXPS system (Figure 1a). ²⁹ The APXPS instrument utilizes a reaction chamber with a base pressure of $<5 \times 10^{-7}$ Pa and the ability to backfill the entire chamber with hydrogen gas during data collection. The reaction chamber is separated from the multistage differentially pumped electrostatic focusing lens system and electron spectrometer by a 300 μ m diameter cone aperture to enable XPS data collection at pressures up to ca. 200 Pa (Figure 1a,b). The sample position was adjusted to the focal point of the X-rays (600 μ m below the aperture) by optimizing the intensity of a photoemission peak. A monochromatized Al K α X-ray

source ($h\nu = 1486.6 \text{ eV}$), focused to a ca. 300 μm diameter spot size and fixed at 55° from the sample normal, was used for acquiring XPS spectra. Survey spectra were collected using a pass energy of 50 eV with a dwell time of 100 ms and a step size of 1 eV, as presented in the Supporting Information. Highresolution spectra were collected with a 20 eV pass energy, 250 ms dwell time, 50 meV step size, and sufficient sweeps for decent signal-to-noise, with doubled number of sweeps for data collected at elevated pressure. No effect of plasma ignition on signal noise was noticed. The spectrometer transmission function was estimated by measuring an Ag reference sample and plotting the intensity of each peak vs KE after normalizing the peaks with respect to their respective cross sections. The plotted data were then interpolated to obtain the transmission function, where the values of each measured electron kinetic energy from this study were entered to obtain a transmissionbased sensitivity factor. A standard set of scans would consist of a survey, Cu 2p, O 1s, N 1s, C 1s, B 1s, and valence band, which would total roughly 3600 s of scan time. Sample heating was performed by controlling the power of an infrared laser aimed at the backside of the sample holder. The temperature was monitored in situ with a K-type thermocouple spot-welded to the sample plate.

The first APXPS differential pumping stage is equipped with a quadrupole mass spectrometer for RGA of the reaction chamber environment during hydrogen/plasma exposure (Figure 1a). The secondary electron multiplier was used to improve signal-to-noise RGA scans when the pressure in the first stage was below 10⁻⁴ Pa. A survey analog scan was first collected for a mass-to-charge ratio (m/z) of 1 to 100 Da/e of the background ultrahigh vacuum (UHV), and then during chamber backfilling of 13 Pa H₂, and during the ignited plasma at 13 Pa H₂, all collected with a sweep time of ca. 33.5 s. During each APXPS spectrum scan, with and without ignited plasma, RGA data were collected only for specific masses (m/z)= [2, 16, 18, 28, 32, 40, and 44] Da/e) for increased time resolution, using 100 ms dwell time for each m/z. To differentiate the on-sample reactions from the side (on-wall) reactions, RGA data were collected where no sample was present in front of the cone orifice during plasma.

Plasma was generated in the APXPS by backfilling the analysis chamber to 13 Pa of H2 and applying 1 keV peak-topeak AC voltage (22 kHz) to the in-chamber copper electrode through a high-voltage feedthrough. The power supply was set to a power output of 15 W. The driving copper electrode was located 10 cm from the sample during XPS spectral acquisition well beyond the main visible discharge area (Figure 1b). Therefore, the sample is under remote plasma conditions where the concentration of ions and electrons is low and surface redox reactions are controlled mainly by hydrogen radical species (Figure 1c). This is confirmed by a hydrogen plasma afterglow spectra that exhibit a violet hue, seen in Figure 1b, due to the mixing of H-alpha (H_{α}) and H-beta (H_{β}) Balmer series visible spectral lines of the hydrogen atom at 656 and 486 nm, respectively. An optical emission spectrum of the hydrogen plasma is shown in Figure 1d, where the major atomic recombination peaks H_{α} and H_{β} are seen, in addition to the much lower intensity broad molecular (H₂ Fulcher) band.

Complementary SEM measurements were conducted ex situ in a separate UHV scanning Auger microscopy system (SAM), at a base pressure of $<1\times10^{-7}$ Pa. The typical electron beam parameters were as follows: probe current within 100 pA to 2 nA range depending on the field of view (FOV); beam energy

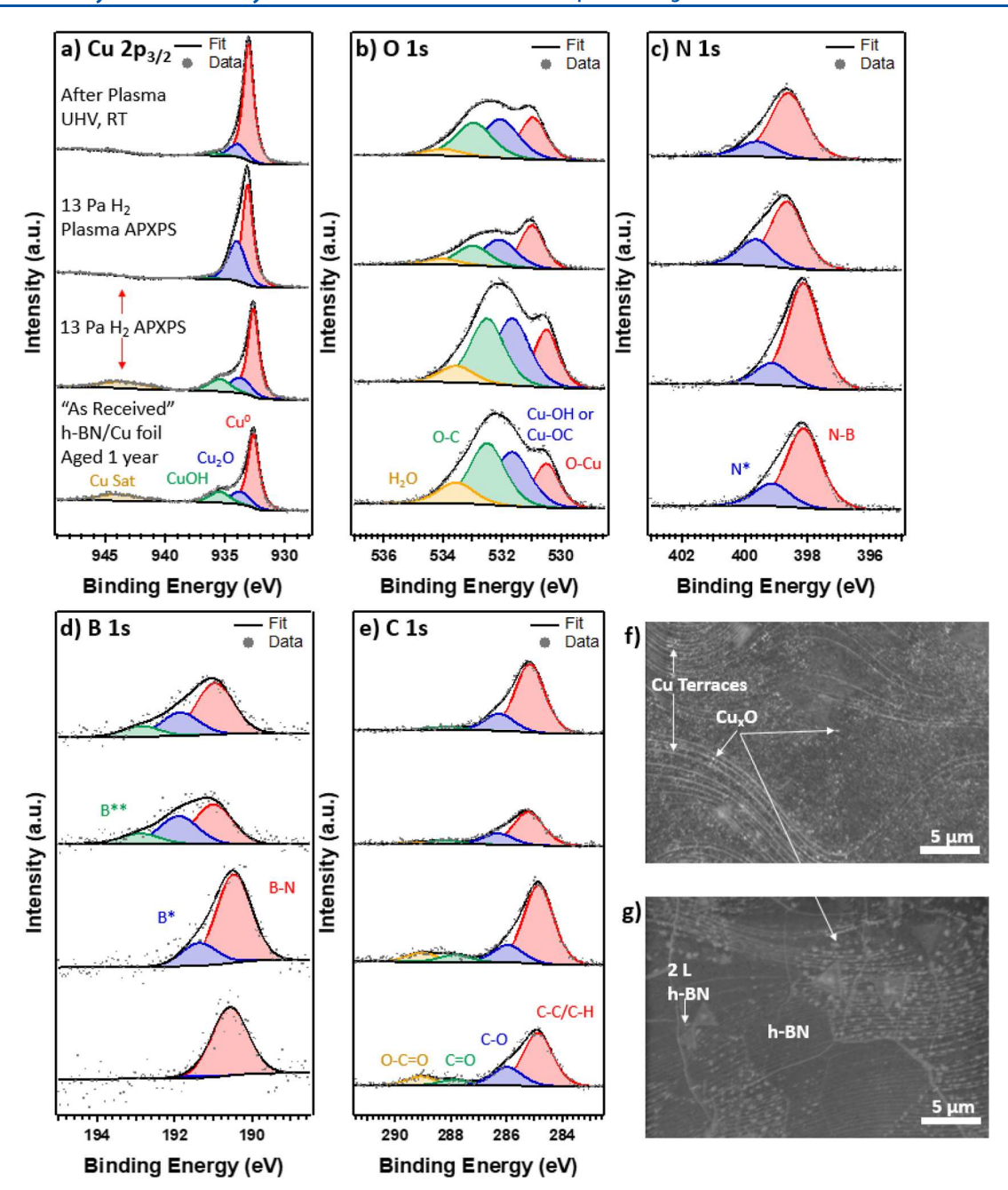


Figure 2. XPS collected for Cu 2p (a), O 1s (b), N 1s (c), and B 1s (d) of "as-received" h-BN/Cu foils (bottom spectra), followed by APXPS in 13 Pa partial pressure of H₂ (middle spectra), and finally during plasma exposure also in 13 Pa partial pressure of H₂ (top spectra), all collected at RT. Representative SEM images of the h-BN/Cu stack collected before (e) and after plasma exposure (f) using nearly the same beam current (2 and 1.5 nA, respectively), beam energy (3 kV), and detector settings.

3 kV; and FOV of ca. 100 nm² to 100 μ m². The sample was angled at 15° toward the analyzer to further enhance the collection efficiency of Auger electrons. SEM images were collected using an in-lens detector, which is sensitive predominately to low-energy secondary electrons. The SAM system also has an XPS chamber for traditional UHV data collection, using a monochromatized Al K α X-ray source ($h\nu$ = 1486.6 eV) focused to ca. 1.5 mm × 2 mm oval spot size and angled 30° from the sample normal. The electron energy analyzer is positioned for 30° electron emission (thus, 90° angle from source to analyzer) and set to a 6.3 mm lens aperture with a 3.3 mm × 11 mm exit slit opening. All survey spectra were collected using 100 eV pass energy, 200 ms dwell

time, 0.5 eV step size, and 2 sweeps. For high-resolution spectra, the pass energy was lowered to 20 eV, with a step size of 50 meV, a dwell time of 300 ms, and sufficient sweeps to achieve a decent signal-to-noise. All XPS spectra were peak fit using a Shirley background and normalized to the lower binding energy baseline to account for occasional changes in X-ray source intensity.

3. RESULTS AND DISCUSSION

The data acquisition flow was the following: after collecting baseline spectra and SEM images of the as-received sample (bottom spectra in Figure 2a—e and Figure 2f, respectively), we backfilled the chamber with 13 Pa partial pressure of H₂

and collected spectra continuously during exposure to molecular hydrogen (middle bottom spectra), leading to an exposure time of roughly 3600 s. At RT, no significant redox chemistry is expected to take place outside of the potential intercalation of H₂. Cu 2p spectra in Figure 2a collected before and after exposure to 13 Pa H₂ show Cu(I) satellite features at a binding energy of ca. 944 eV, in addition to three peak fits of the $2p_{3/2}$ peak, corresponding to metallic Cu⁰ (932.6 eV, red), Cu⁺ copper(I) oxide (933.7 eV, green), and Cu⁺ copper(I) hydroxide (935.4 eV, blue).30 This agrees well with beforeand-after O 1s spectra shown in Figure 2b, where two oxidized Cu peaks are seen at 530.5 eV (red) and 531.6 eV (blue). The lower energy (red) peak corresponds to Cu⁺ copper(I) oxide, while the higher energy (blue) peak is most likely copper(I) hydroxide, 31 although it could also be Cu-bound carbonate species.³² Two additional peaks are also seen corresponding to adventitious carbon species (532.5 eV, green) and adsorbed water 533.7 eV (orange). These two higher energy peak intensities are likely affected by d-band-to-Fermi level excitations that lower the O 1s energy of the Cu_xO-based electrons, providing a broadened peak at ca. 533 eV that will overestimate the intensity of the adventitious species.³³ In our case, the main focus is the change in relative peak ratios of the two cuprous oxide peaks to the adventitious contamination peaks and the change in overall total oxide content. Ultimately, RT exposure to molecular H₂ at 13 Pa shows no clear evidence of reduction of the Cu substrate, with the primary difference being a slight increase in adventitious carbon and a decrease in adsorbed water, which can be explained by a change in vapor equilibrium with the introduction of H₂ gas. Similarly, adsorption of other volatile adventitious species from chamber outgassing by introducing H2 explains the increase in carbon also seen in C 1s.

Virtually no change is seen in the N 1s (Figure 2c) before and after exposure to molecular H_2 , where two peaks can be fit, corresponding to N-B (398.1 eV, red) and N* (399.1 eV, green). The shoulder peak (N*) arises from defects in the BN layer that can be attributed to domain boundaries, multilayers, and/or differences in h-BN/Cu interaction where a stronger interaction leads to charge transfer and creates a shift to higher binding energy. 19,34 Intercalation of molecules like CO can cause the XPS binding energy to shift even further as the h-BN/substrate interaction changes due to intercalation.³⁴ This phenomenon is also present for the B 1s and can explain the change seen in Figure 2d, where initially a single peak fit corresponding to B-N (190.5 eV) then develops a shoulder peak seen at 191.4 eV (B*) after H₂ exposure. In this case, exposure to, and intercalation of, H2 can weaken the interaction of B-Cu, or additionally H2 intercalation between multilayer islands (triangles seen in Figure 2e,f) can create a similar peak shift. In our case, we use only one additional peak fit to account for these peak shifts in N 1s and B 1s, although there are likely multiple peaks with similar energies that create this shoulder feature.

Following molecular exposures, we ignited a cold plasma described in the experimental section where the discharge source was positioned 10 cm away from the sample to expose the sample predominantly to hydrogen radicals (remote plasma conditions). Additional experiments (not shown here) indicated that direct plasma exposure can cause the h-BN single layer to be etched away by hydrogen ions within a few hundred seconds. Instead, under a gentle remote plasma, partially thermalized H radical species become the primary

species interacting with the sample, opposite energetic ions, and electrons under direct plasma exposure that can etch h-BN

In Figure 2a, a clear loss in Cu 2p satellites takes place during operando spectra acquisition under plasma exposure (top spectra), in addition to the removal of the Cu_xO shoulder, signifying a clear reduction of the Cu although some Cu⁺ component remains. The O 1s in Figure 2b shows a decrease in the relative ratios between the adventitious species and the oxidized Cu from the substrate, confirming that the plasma can also interact with and "clean" the surface, although these adventitious species can be redeposited to the surface rather quickly at this pressure upon the quenching of the plasma, seen by the increase in peak intensities for the spectra collected at RT and UHV after plasma exposure. The N 1s remains mostly the same, although it shows an increase in the ratio of N-B to N*, while the B 1s shows a significant increase in the secondary higher energy peak, again suggesting that intercalative species may be affecting the interaction between B and the Cu substrate. Additionally, the presence of a higher energy peak (B**) becomes clear, which could be related to oxidized boron. However, there is no clear indication of oxidized boron species in the O 1s spectra, which would be expected at ca. 534 eV, and while the adsorbed water peak is near this energy, the peak intensity goes down upon plasma exposure; thus, oxidation of B is most likely not taking place during exposure to a reducing plasma. It is possible that this increase in B* and B** can be from newly formed defects in the BN lattice as a similar increase in the N* component of the N 1s spectra is seen. Most likely, these defects are from islands of exposed 2L h-BN (seen in SEM of Figure 2), where B-H or N-H bonds are formed from reactions with plasma radicals. Overall, there is an adequate remainder of N-B and B-N clearly seen in the N 1s and B 1s, which suggests that an overlayer is still mostly present and potentially repairable by annealing.

After exposure to plasma, we purged the chamber to UHV and cooled it to RT for collection of spectra again. Upon cooling, we see the readsorption of some O and C species that were removed during plasma exposure. Also, Cu 2p shows even more reduction, as the sample was still being exposed to plasma for the collection of the remainder of components (Cu 2p was collected first). Not much change is seen to the B or N 1s after quenching the plasma, other than a slight decrease in B and N*, which could be related to desorption of H after returning to UHV.

To gain a better understanding of the XPS results, we utilized the Fadley method for calculating XPS atomic ratios with the overlayer model,³⁵ where we can determine how the B 1s, N 1s, O 1s, and C 1s change with respect to the Cu 2p substrate peak. Using the spectrometer geometry mentioned in the Methods section, calculating the transmission function with an Ag reference (also mentioned in the Methods section), assuming negligible differences in spectrometer detection efficiency, and data tables for inelastic mean free paths³⁶ along with photoabsorption cross sections,³⁷ we can calculate each ratio shown in Table 1. The total B/N is expected to be less than 1 as the incorporation of O combined with the low photoabsorption cross section of B 1s with Al klpha X-rays leads to an underestimation of the B 1s. As the spectra suggest, the overall O content remains mostly the same after 3600 s exposure to 13 Pa H₂. The change in equilibrium pressure in the chamber and desorption of adsorbed water explains the

Table 1. Atomic Ratios Were Calculated for B 1s, N 1s, C 1s, and O 1s with Respect to (wrt) Cu 2p for Slightly Oxidized h-BN/Cu As-Received, During APXPS at 13 Pa H₂, During Plasma-XPS at 13 Pa H₂, and After Plasma Exposure^a

	B 1s	O 1s	N 1s	C 1s
as-rec	0.9 ± 0.5	5.2 ± 0.2	1.6 ± 0.2	3.8 ± 0.5
13 Pa H ₂	1.2 ± 0.3	4.8 ± 0.1	1.5 ± 0.2	4.1 ± 0.3
13 Pa H ₂ plasma	0.8 ± 0.2	1.8 ± 0.1	1.0 ± 0.1	1.6 ± 0.2
after plasma	1.0 ± 0.2	2.9 ± 0.1	1.1 ± 0.1	3.3 ± 0.3

"A Monte Carlo regression was executed by repeatedly adding noise for 200 simulations where the artificial data were fit, providing a standard deviation for area values that were propagated to the error of the calculated ratios provided in the table.

slight decrease from 5.2 to 4.8 in O 1s and the increase in the very surface-sensitive B 1s signal from 0.9 to 1.2, while the total N 1s remains mostly the same. The C 1s value slightly increases, likely due to chamber outgassing with introduction of the H₂ overpressure. During plasma exposure, the total O 1s and C 1s decrease by roughly two-thirds of the signal during molecular H₂ exposure, while the total N 1s and B 1s decrease by only 1/3. The decrease in N 1s and B 1s is also anticipated as the reduced Cu and removal of adventitious species enhance the substrate signal that all values are referenced to. Still, the N/B ratio remains at ≈0.7 from molecular H₂ to plasma exposure, but once the sample is returned to UHV and RT after plasma, the ratio becomes ≈0.9, much closer to the expected 1:1 ratio. The 0.7 ratio seen during H2 APXPS and plasma-XPS is likely underestimated due to attenuation in the gas phase in both measurements, along with an additional biasing effect from the plasma potential, which is energydependent and difficult to account for in these atomic ratio calculations.

Interestingly, we observed a noticeable shift of ca. 0.5 eV to a higher binding energy for all peaks during *operando* XPS under plasma conditions. Correlative change in binding energies could not be explained by intercalation phenomena³⁴ since it would lead to weakening interaction with the substrate and lowering the BE. In addition, a similar shift occurs also in the

Cu 2p and valence band spectra of the substrate foil, which should still be well grounded, while additionally not shifting back to the initial energy upon quenching of the plasma. Since the peaks do not shift back after plasma exposure, this shift cannot be related to an interplay between surface charging and plasma potential. Instead, the shift presumably is an electronic effect as the removal of oxygen at the h-BN/Cu interface changes the band offset and thus lowers the referenced Fermi level. A related reverse effect was seen during oxidation of pristine h-BN/Cu(111) where a peak shift to lower BE is seen upon oxidation.²¹ This same behavior has also been seen for the Co/h-BN interface exhibiting p-type band bending.³⁸ We have to note, however, that we do observe strong plasmainduced binding energy shifts on dielectric and semiconductor surfaces due to surface charging in a plasma sheath. These effects are fully reversible and are the subject of current studies.

Typical areas of SEM images were also collected ex situ before and after exposure to plasma presented in Figure 2f,g, respectively. Prior to exposure, as received, the slightly oxidized h-BN/Cu sample surface is covered with oxidized Cu clusters (bright spots) appearing on an otherwise smooth h-BN/Cu gray background. Oxidized spots densely decorate Cu staircase valley edges. Some 2L multilayer h-BN can also be observed as characteristic triangles. After plasma exposure, the fraction of the pristine (gray) h-BN/Cu area noticeably increases with a concomitant reduction in the density of the oxidized (bright) clusters and an overall decrease of O 1s peak intensity. Simple particle analysis of the before-and-after SEM images of the oxidized Cu fraction corroborates with XPS observations, confirming that the plasma is reacting with the C/O species and "cleaning"/reducing the h-BN/Cu surface, while the BN seems to remain intact under our remote plasma conditions. It is not surprising that the surface contamination above the h-BN layer decreases with exposure to plasma, but the clear change in the Cu peak from XPS and evidence still of h-BN wrinkles and multilayer triangles from SEM after exposure demonstrate that the plasma is also interacting with the confined interface underneath h-BN. Unfortunately, we cannot state for certain if the h-BN layer remains unchanged at the nanoscale level without a more rigorous structural analysis.

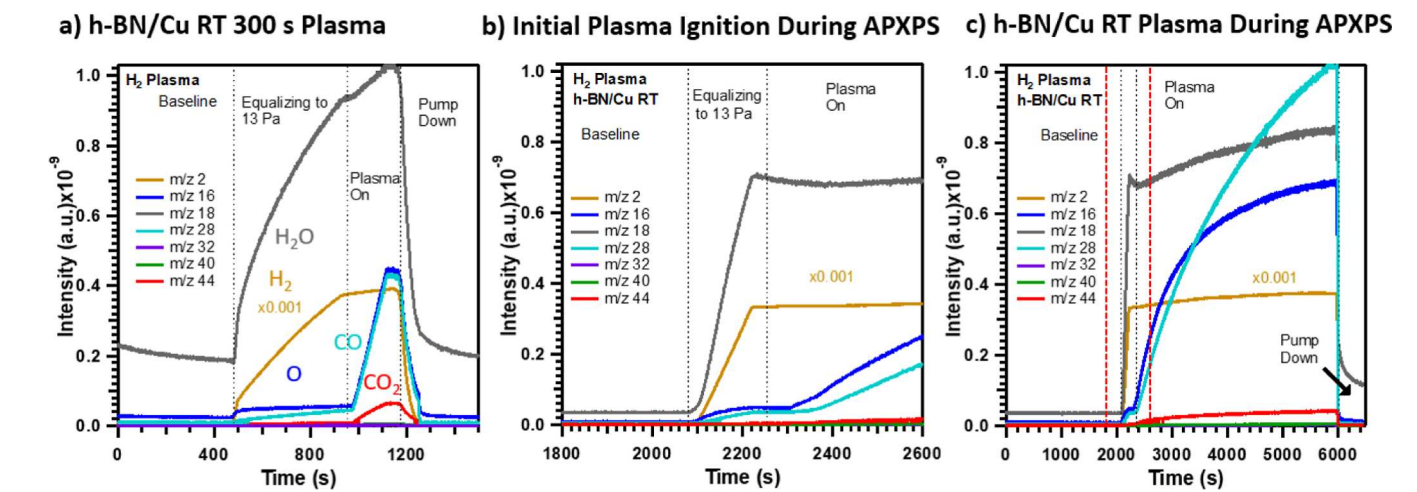


Figure 3. RGA mass spectra collected during hydrogen remote plasma exposure for 300 s with the sample moved away from the "sniffing" cone (a) and during plasma-XPS (b) for 3600 s. A zoomed-in slice on a similar time scale is shown in (b) and highlighted by red dotted lines with the full-time range shown in (c). Gray dotted lines signify changes in the chamber ambient. H_2 signal (m/z = 2 Da/e, golden curve) is reduced by a factor of 10^{-3} for scaling.

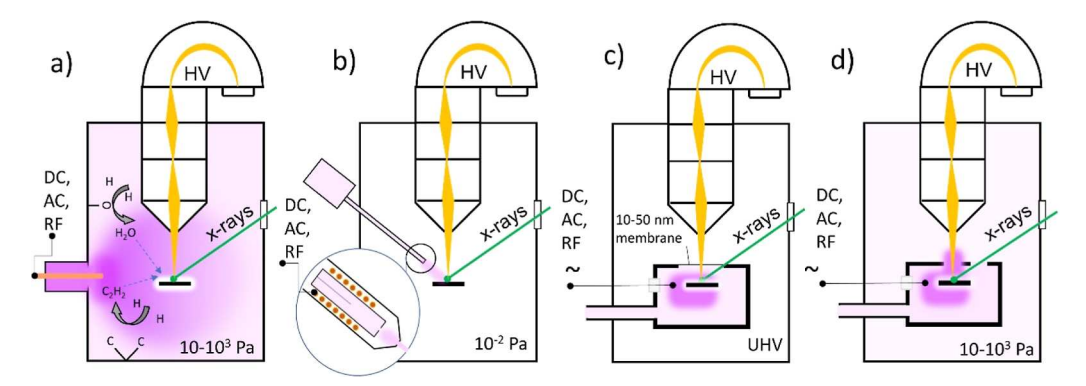


Figure 4. Current (a) and proposed (b-d) experimental setups for plasma-XPS. Running global plasma in a standard APXPS analytical chamber may contaminate the sample of interest due to parasitic plasma—wall reactions (a). (Pulsed) microjet plasma (b) eliminates this problem and can also be easily combined with liquid jet APXPS systems and plasma reaction kinetics studies; (c) membrane-based microchamber with microdischarge inside can, in principle, operate under UHV conditions but mechanical and plasma robustness limitations for ca. 50 nm thick membranes require the use of tender or hard X-rays to ensure sufficient membrane electron transparency; (d) open microchamber design with precoated and well-cleaned walls combines advantages of (b) and (c) and is fully compatible with standard APXPS systems.

However, since we do not see any clear evidence of characteristic etching pits or triangular island erosion following plasma exposure, we can attribute the XPS changes to the N and B 1s after plasma exposure to be primarily from reducing the oxide at the h-BN/Cu interface. Hydrogenation of dangling bonds at domain boundaries could take place but is not easily identifiable with XPS due to the inability to measure hydrogen XPS.

We now discuss the necessity of the operando plasma-XPS studies and one of the challenges of in-chamber plasma-XPS. To get a sense of potential reactions occurring on the sample, we used the RGA connected to the first APXPS pumping stage, similar to a prior APXPS experiment, 39 which utilizes the cone orifice as a "sniffing" probe of the plasma-induced reaction products originating at the h-BN/Cu sample surface. Since the sample-to-orifice distance was in the same order of magnitude as the average molecular mean free path at 13 Pa of hydrogen (our standard plasma conditions), the assumption was that a significant fraction of the molecules entering the cone orifice would experience at least a single collision with the sample surface and would be related to the products of plasmainduced surface reactions. To test the feasibility of this approach and to discriminate between possible artifacts, we collected RGA spectra during running plasma conditions when a sample was (i) moved far away from the optimal "sniffing" conditions and (ii) in front of the cone orifice.

Figure 3 shows temporal evolutions of ion currents for few major molecular components during exposure to plasma for 300 s (a) and during the plasma APXPS collection (b) at RT for 3600 s. Dotted lines in the figure separate between the different chamber environments, starting with an initial baseline, after equalizing to 13 Pa partial pressure of H₂, when the plasma is switched on, and during pumping down as the chamber is purged. Figure 3c shows red dotted lines, which highlight the zoomed-in time scale shown in Figure 3b. During the 300 s exposure in Figure 3a, the sample was moved away from the cone and is primarily defined by the changes in gas composition inside the analytical chamber upon plasma application. Initially, as the H₂ is backfilled into the chamber, we see an uptake of all masses, which is common for APXPS as the increase of the background pressure leads to outgassing from the chamber walls. 40 As the plasma is ignited, an immediate increase in the O (m/z 16 Da/e, blue), CO (m/z 28 Da/e, aqua), and CO₂ (m/z 44 Da/e, red) signals can be observed directly corresponding with the plasma onset. A slight increase in the H₂O concentration (m/z 18 Da/e, gray) is also seen. Note that no significant changes can be seen for H₂ (m/z = 2 Da/e, golden curve).

We interpret the observed results as plasma-induced reactions with water and hydrocarbon molecules adsorbed at the chamber walls, the effect of which is well known in the plasma community as plasma reactor wall conditioning. Note that qualitatively similar responses for all the same molecular components can be observed during the APXPS measurements under plasma conditions when the sample is in front of and in proximity to the "sniffing" cone (Figure 3b). This fact manifests two challenges: (i) the important and potentially parasitic role of the side-wall reactions on the surface chemistry of the sample of interest due to cross-contamination and (ii) the need for understanding and optimization of sampleselective mass spectroscopy in a global plasma environment. Indeed, when the sample is placed directly in front of the cone, the pumping efficiency of the chamber through the cone is noticeably reduced. The observed kinetics in mass spectra becomes a complex function of the true surface reactions, molecule-specific orifice conductance, and sample/orifice temperature due to its possible Joule-Thomson cooling. These effects should not be significant in that they completely misrepresent our hydrogen plasma results, but they generally could make interpretation more challenging if one intended to draw surface reaction paths and kinetics from the mass spectroscopy data and compare this to XPS measurements. Some of the potentially useful experimental solutions are proposed in the next section.

4. CONCLUSIONS AND OUTLOOK

To summarize, we demonstrated that good-quality XPS spectra can be collected while running plasma in the APXPS chamber. Using CVD-grown h-BN monolayer Cu foil, we were able to monitor the reduction of the oxidized Cu_xO clusters and patches under remote plasma conditions, without noticeable destruction of the h-BN overlayer. We also observed that the operando plasma-measured core level energies of the h-BN/Cu system exhibit the shift which provides clear evidence of the reduction of oxide at the h-BN/Cu interface. On the other hand, poorly conducting samples exhibit significant (up to tens

of eV) but reversible XPS binding energy shifts when exposed to a plasma environment due to surface charge buildup.

Furthermore, we emphasize that care must be taken in interpreting the plasma-induced reactions at the sample surface since the global plasma in the standard APXPS induces numerous parasitic reactions at the chamber walls that, in turn, can alter the sample surface (Figure 4a). These side-reactions are an important component of real-world plasma environments, and plasma XPS metrology is an ideal platform for their better studies. Potential solutions to differentiate between the true sample and parasitic chamber wall plasma-induced reactions would be localization of the plasma around the sample using continuous or pulsed plasma microjets (Figure 4b; can also be combined with liquid microjet APXPS designs) or employing thoroughly degassed small size sample enclosures with a microplasma discharge inside (Figure 4c,d). These could be completely sealed ca. 50 nm thick membrane-based microchambers 41 (requires tender or hard X-rays for sufficient photoelectron transparency) or ones with open photon-in and electron-out orifices. Such hardware, in principle, is already available at some APXPS setups and requires only minor customization for (micro-) PS incorporation. 1,42,43

Overall, plasma-XPS is a new emerging metrology platform that will greatly complement existing plasma chemistry studies. The main advantage of this operando method is the ability to detect short-living and/or fast-desorbing/diffusing reaction plasma-induced intermediates that are hard or impossible to interrogate using a standard before-and-after approach. When coupled with mass spectrometry, optical, and conductometric/ electrochemical measurements, plasma-XPS can become the metrology of choice for a comprehensive study to monitor complex plasma-solid or plasma-liquid interfaces, including biomedical systems. A good example is sensitive monitoring of industrially relevant plasma-assisted deposition or etching processes, which are often pulsed and temperature modulated. In addition, plasma-XPS drastically improves the effectiveness of standard plasma-surface interaction studies, where, for example, thermal cycling can be done under plasma exposure without multiple lengthy sample transfers (or switching) between analytical and plasma chambers (operation modes). With the current level of APXPS instrumentation development, the apparent application areas of plasma-XPS in semiconductor manufacturing and process control, biomedical diagnostics and treatment, aerospace materials development, environmental remediation, plasma catalysis, and many others can be envisioned. Finally, the goal of this work is to not only assist current fields but also possibly inspire new directions for plasma-XPS metrology.

ASSOCIATED CONTENT

Data Availability Statement

The data both presented and not presented in this report, which support the findings of this study, are available upon reasonable request.

Supporting Information

The Supporting Information is available free of charge at https://pubs.acs.org/doi/10.1021/acs.jpcc.4c00253.

Survey XPS spectra corresponding to XPS presented in Figure 2, along with a brief explanation of the XPS survey measurement parameters (PDF)

AUTHOR INFORMATION

Corresponding Authors

J. Trey Diulus — Nanoscale Device Characterization Division, PML, NIST, Gaithersburg, Maryland 20899, United States; orcid.org/0000-0001-8675-8581; Email: john.diulus@nist.gov

Andrei Kolmakov — Nanoscale Device Characterization Division, PML, NIST, Gaithersburg, Maryland 20899, United States; orcid.org/0000-0001-5299-4121; Email: andrei.kolmakov@nist.gov

Authors

Andrew E. Naclerio – Department of Chemical and Biomolecular Engineering, Vanderbilt University, Nashville, Tennessee 37212, United States

Jorge Anibal Boscoboinik — Center for Functional Nanomaterials, Brookhaven National Laboratory, Upton, New York 11973, United States; © orcid.org/0000-0002-5090-7079

Ashley R. Head — Center for Functional Nanomaterials, Brookhaven National Laboratory, Upton, New York 11973, United States; © orcid.org/0000-0001-8733-0165

Evgheni Strelcov – Nanoscale Device Characterization Division, PML, NIST, Gaithersburg, Maryland 20899, United States

Piran R. Kidambi — Department of Chemical and Biomolecular Engineering, Vanderbilt University, Nashville, Tennessee 37212, United States; Department of Mechanical Engineering, Vanderbilt University, Nashville, Tennessee 37212, United States; Vanderbilt Institute of Nanoscale Sciences and Engineering, Nashville, Tennessee 37212, United States; orcid.org/0000-0003-1546-5014

Complete contact information is available at: https://pubs.acs.org/10.1021/acs.jpcc.4c00253

Author Contributions

The manuscript was written through contributions of all authors. All of the authors approved the final version of the manuscript. Conceptualization: A.K., J.T.D. Methodology: J.T.D., A.E.N., J.A.B., A.R.H., E.S., P.R.K., A.K. Investigation: J.T.D., J.A.B., A.K. Visualization: J.T.D., A.K. Funding acquisition: J.T.D., J.A.B., A.R.H., P.R.K., A.K. Project administration: A.K. Supervision: A.K. Writing—original draft: A.K., J.T.D. Writing—review and editing: E.S., A.R.H., J.A.B., A.E.N., P.R.K.

Notes

Certain equipment, instruments, software, or materials, commercial or noncommercial, are identified in this paper to specify the experimental procedure adequately. Such identification is not intended to imply recommendation or endorsement of any product or service by NIST, nor is it intended to imply that the materials or equipment identified are necessarily the best available for the purpose.

The authors declare no competing financial interest.

ACKNOWLEDGMENTS

We acknowledge Glenn Holland and David Rutter (both at NIST) for their technical support. Reviewing and comments from J. Campbell, E. Secula, Ch. Hacker, S. Robey (all from NIST), and M. Kiskinova (ELETTRA) are greatly appreciated. This research used the Proximal Probes Facility of the Center for Functional Nanomaterials (CFN), which is a U.S.

Department of Energy Office of Science User Facility, at Brookhaven National Laboratory under Contract DE-SC0012704. P.R.K. acknowledges funding support via the NSF CAREER Award 1944134 and DOE Early Career Research Program Award DE-SC0022915.

REFERENCES

- (1) Dupuy, R.; Richter, C.; Winter, B.; Meijer, G.; Schlögl, R.; Bluhm, H. Core Level Photoelectron Spectroscopy of Heterogeneous Reactions at Liquid-Vapor Interfaces: Current Status, Challenges, and Prospects. *J. Chem. Phys.* **2021**, *154*, 060901.
- (2) Salmeron, M. From Surfaces to Interfaces: Ambient Pressure XPS and Beyond. *Top. Catal.* **2018**, *61*, 2044–2051.
- (3) Nguyen, L.; Tao, F. F.; Tang, Y.; Dou, J.; Bao, X. J. Understanding Catalyst Surfaces During Catalysis through near Ambient Pressure X-Ray Photoelectron Spectroscopy. *Chem. Rev.* **2019**, *119*, 6822–6905.
- (4) Schnadt, J.; Knudsen, J.; Johansson, N. Present and New Frontiers in Materials Research by Ambient Pressure X-ray Photoelectron Spectroscopy. *J. Phys.: Condens. Matter* **2020**, 32, 413003.
- (5) Bronold, F.; Rasek, K.; Fehske, H. Electron Microphysics at Plasma-Solid Interfaces. J. Appl. Phys. 2020, 128, 180908.
- (6) Vinchon, P.; Asadollahi, S.; Coté, C.; Marcet, S.; Atallah, S.; Dessureault, E.; Chicoine, M.; Sarkissian, A.; Leonelli, R.; Roorda, S.; et al. In-Plasma Analysis of Plasma-Surface Interactions. *Rev. Sci. Instrum.* 2023, 94, 083305.
- (7) Donnelly, V.; Guha, J.; Stafford, L. Critical Review: Plasma-Surface Reactions and the Spinning Wall Method. *J. Vac. Sci. Technol., A* **2011**, 29, 010801.
- (8) Operando NAP-XPS Study of Plasma-Enhanced Surface Reactions. *Application Note #230401*; SPECS Surface Nano Analysis GmbH, 2023.
- (9) Dong, B.; Driver, M. S.; Emesh, I.; Shaviv, R.; Kelber, J. A. Surface Chemistry and Fundamental Limitations on the Plasma Cleaning of Metals. *Appl. Surf. Sci.* **2016**, *384*, 294–297.
- (10) Vandencasteele, N.; Reniers, F. Plasma-Modified Polymer Surfaces: Characterization Using XPS. J. Electron Spectrosc. Relat. Phenom. 2010, 178–179, 394–408.
- (11) Naclerio, A. E.; Kidambi, P. R. A Review of Scalable Hexagonal Boron Nitride (h-BN) Synthesis for Present and Future Applications. *Adv. Mater.* **2022**, *35*, 2207374.
- (12) Moon, S.; Kim, J.; Park, J.; Im, S.; Kim, J.; Hwang, I.; Kim, J. K. Hexagonal Boron Nitride for Next-Generation Photonics and Electronics. *Adv. Mater. Interfaces* **2023**, *35*, 2204161.
- (13) Roy, S.; Zhang, X.; Puthirath, A. B.; Meiyazhagan, A.; Bhattacharyya, S.; Rahman, M. M.; Babu, G.; Susarla, S.; Saju, S. K.; Tran, M. K.; et al. Structure, Properties and Applications of Two-Dimensional Hexagonal Boron Nitride. *Adv. Mater.* **2021**, *33*, 2101589.
- (14) Sasama, Y.; Komatsu, K.; Moriyama, S.; Imura, M.; Teraji, T.; Watanabe, K.; Taniguchi, T.; Uchihashi, T.; Takahide, Y. High-Mobility Diamond Field Effect Transistor with a Monocrystalline h-BN Gate Dielectric. *APL Mater.* **2018**, *6*, 111105.
- (15) Li, L. H.; Xing, T.; Chen, Y.; Jones, R. Boron Nitride Nanosheets for Metal Protection. *Adv. Mater. Interfaces* **2014**, *1*, 1300132.
- (16) Lo, C.-L.; Helfrecht, B. A.; He, Y.; Guzman, D. M.; Onofrio, N.; Zhang, S.; Weinstein, D.; Strachan, A.; Chen, Z. Opportunities and Challenges of 2D Materials in Back-End-of-Line Interconnect Scaling. *J. Appl. Phys.* **2020**, *128*, 080903.
- (17) Uwanno, T.; Hattori, Y.; Taniguchi, T.; Watanabe, K.; Nagashio, K. Fully Dry PMMA Transfer of Graphene on h-BN Using a Heating/Cooling System. 2D Mater. 2015, 2, 041002.
- (18) Vlassiouk, I.; Smirnov, S.; Puretzky, A.; Olunloyo, O.; Geohegan, D. B.; Dyck, O.; Lupini, A. R.; Unocic, R. R.; Meyer, H. M., III; Xiao, K.; et al. Armor for Steel: Facile Synthesis of Hexagonal Boron Nitride Films on Various Substrates. *Adv. Mater. Interfaces* **2023**, *11*, 2300704.

- (19) Kidambi, P. R.; Blume, R.; Kling, J.; Wagner, J. B.; Baehtz, C.; Weatherup, R. S.; Schloegl, R.; Bayer, B. C.; Hofmann, S. In Situ Observations During Chemical Vapor Deposition of Hexagonal Boron Nitride on Polycrystalline Copper. *Chem. Mater.* **2014**, *26*, 6380–6392.
- (20) Scardamaglia, M.; Boix, V.; D'Acunto, G.; Struzzi, C.; Reckinger, N.; Chen, X.; Shivayogimath, A.; Booth, T.; Knudsen, J. Comparative Study of Copper Oxidation Protection with Graphene and Hexagonal Boron Nitride. *Carbon* **2021**, *171*, 610–617.
- (21) Diulus, J. T.; Novotny, Z.; Dongfang, N.; Beckord, J.; Al Hamdani, Y.; Comini, N.; Muntwiler, M.; Hengsberger, M.; Iannuzzi, M.; Osterwalder, J. h-BN/Metal-Oxide Interface Grown by Intercalation: A Model System for Nano-Confined Catalysis. *J. Phys. Chem. C* 2024, 128, 5156–5167.
- (22) Kidambi, P. R.; Chaturvedi, P.; Moehring, N. K. Subatomic Species Transport through Atomically Thin Membranes: Present and Future Applications. *Science* **2021**, *374*, No. eabd7687.
- (23) Wei, M.; Fu, Q.; Wu, H.; Dong, A.; Bao, X. Hydrogen Intercalation of Graphene and Boron Nitride Monolayers Grown on Pt (111). *Top. Catal.* **2016**, *59*, 543–549.
- (24) He, L.; Wang, H.; Chen, L.; Wang, X.; Xie, H.; Jiang, C.; Li, C.; Elibol, K.; Meyer, J.; Watanabe, K.; et al. Isolating Hydrogen in Hexagonal Boron Nitride Bubbles by a Plasma Treatment. *Nat. Commun.* **2019**, *10*, 2815.
- (25) Konyashin, I.; Khvostov, V.; Babaev, V.; Guseva, M.; Bill, J.; Aldinger, F. The Influence of Excited Hydrogen Species on the Surface State of sp²-Hybridized Boron Nitride. *Diamond Relat. Mater.* **1999**, *8*, 2053–2058.
- (26) Koswattage, K. R.; Shimoyama, I.; Baba, Y.; Sekiguchi, T.; Nakagawa, K. Selective Adsorption of Atomic Hydrogen on a h-BN Thin Film. *J. Chem. Phys.* **2011**, *135*, 014706.
- (27) Zhang, H.; Feng, P. Controlling Bandgap of Rippled Hexagonal Boron Nitride Membranes Via Plasma Treatment. *ACS Appl. Mater. Interfaces* **2012**, *4*, 30–33.
- (28) Reinke, P.; Oelhafen, P.; Feldermann, H.; Ronning, C.; Hofsäss, H. Hydrogen-Plasma Etching of Ion Beam Deposited c-BN Films: An In Situ Investigation of the Surface with Electron Spectroscopy. *J. Appl. Phys.* **2000**, *88*, 5597–5604.
- (29) Eads, C. N.; Zhong, J.-Q.; Kim, D.; Akter, N.; Chen, Z.; Norton, A. M.; Lee, V.; Kelber, J. A.; Tsapatsis, M.; Boscoboinik, J. A.; et al. Multi-Modal Surface Analysis of Porous Films under Operando Conditions. *AIP Adv.* **2020**, *10*, 085109.
- (30) Biesinger, M. C.; Lau, L. W. M.; Gerson, A. R.; Smart, R. S. C. Resolving Surface Chemical States in XPS Analysis of First Row Transition Metals, Oxides and Hydroxides: Sc, Ti, V, Cu and Zn. Appl. Surf. Sci. 2010, 257, 887–898.
- (31) Deroubaix, G.; Marcus, P. X-ray Photoelectron Spectroscopy Analysis of Copper and Zinc Oxides and Sulphides. *Surf. Interface Anal.* **1992**, *18*, 39–46.
- (32) Wagner, C. D.; Zatko, D. A.; Raymond, R. H. Use of the Oxygen KLL Auger Lines in Identification of Surface Chemical States by Electron Spectroscopy for Chemical Analysis. *Anal. Chem.* **1980**, 52, 1445–1451.
- (33) Hayashida, K.; Tsuda, Y.; Yamada, T.; Yoshigoe, A.; Okada, M. Revisit of XPS Studies of Supersonic O_2 Molecular Adsorption on Cu(111): Copper Oxides. ACS Omega 2021, 6, 26814–26820.
- (34) Ng, M. L.; Shavorskiy, A.; Rameshan, C.; Mikkelsen, A.; Lundgren, E.; Preobrajenski, A.; Bluhm, H. Reversible Modification of the Structural and Electronic Properties of a Boron Nitride Monolayer by Co Intercalation. *ChemPhysChem* **2015**, *16*, 923–927.
- (35) Fadley, C. Basic Concepts of X-ray Photoelectron Spectroscopy; Academic Press: London, England, UK, 1978; Vol. 2; pp 1–156.
- (36) Tanuma, S.; Powell, C. J.; Penn, D. R. Calculations of Electron Inelastic Mean Free Paths. IX. Data for 41 Elemental Solids over the 50 eV to 30 keV Range. *Surf. Interface Anal.* **2011**, *43*, 689–713.
- (37) Yeh, J. J.; Lindau, I. Atomic Subshell Photoionization Cross Sections and Asymmetry Parameters: $1 \le Z \le 103$. Atomic Data Nucl. Data Tables 1985, 32, 1–155.

- (38) Driver, M. S.; Beatty, J. D.; Olanipekun, O.; Reid, K.; Rath, A.; Voyles, P. M.; Kelber, J. A. Atomic Layer Epitaxy of h-BN(0001) Multilayers on Co(0001) and Molecular Beam Epitaxy Growth of Graphene on h-BN(0001)/Co(0001). *Langmuir* **2016**, 32, 2601–2607.
- (39) Diulus, J. T.; Elzein, R.; Addou, R.; Herman, G. S. Surface Chemistry of 2-Propanol and O_2 Mixtures on $SnO_2(110)$ Studied with Ambient-Pressure X-ray Photoelectron Spectroscopy. *J. Chem. Phys.* **2020**, 152, 054713.
- (40) Trotochaud, L.; Head, A. R.; Karslioglu, O.; Kyhl, L.; Bluhm, H. Ambient Pressure Photoelectron Spectroscopy: Practical Considerations and Experimental Frontiers. *J. Phys.: Condens. Matter* **2017**, 29, 053002.
- (41) Tselev, A.; Fagan, J.; Kolmakov, A. In-Situ Near-Field Probe Microscopy of Plasma Processing. *Appl. Phys. Lett.* **2018**, *113*, 263101.
- (42) Amati, M.; Bonanni, V.; Braglia, L.; Genuzio, F.; Gregoratti, L.; Kiskinova, M.; Kolmakov, A.; Locatelli, A.; Magnano, E.; Matruglio, A.; et al. Operando Photoelectron Emission Spectroscopy and Microscopy at Elettra Soft X-ray Beamlines: From Model to Real Functional Systems. J. Electron Spectrosc. Relat. Phenom. 2022, 257, 146902.
- (43) Masuda, T. Various Spectroelectrochemical Cells for In Situ Observation of Electrochemical Processes at Solid-Liquid Interfaces. *Top. Catal.* **2018**, *61*, 2103–2113.